UNIVERSITY OF
LATVIA

Summary of
Doctoral Thesis

Janis Cipa

INTEGRATED MICROFLUIDIC DEVICE FOR RAPID MIXING AND MAGNETIC SEPARATION OF PROSTATE CANCER EXTRACELLULAR VESICLES

Riga 2025

UNIVERSITY OF
LATVIA

FACULTY OF SCIENCE AND TECHNOLOGY

Janis Cipa

INTEGRATED MICROFLUIDIC DEVICE FOR RAPID MIXING AND MAGNETIC SEPARATION OF PROSTATE CANCER EXTRACELLULAR VESICLES

SUMMARY OF THE DOCTORAL THESIS

Submitted for the degree of Doctor of Engineering and Technology
Field of Materials Science
Subfield of Materials Physics

Riga 2025

The doctoral thesis was carried out at the Institute of solid state physics, University of Latvia, from year 2021 to 2025.

The creation of this thesis was supported by Camart2 project No 1.1.1.4/17/I/002, European Regional Development Fund (ERDF), No 1.1.1.1/20/A/045 and Latvian Council of Science project VPP-EM-FOTONIKA-2022/1-0001.

Form of the thesis: dissertation in the field of materials science, subfield of materials physics.

Supervisor: *Dr. phys.* **Roberts Rimsa**, Institute of Solid State Physics University of Latvia.

Reviewers:

Aivars Vembris, *Dr. phys.,* lead researcher, Institute of Solid State Phyiscs;
Guntars Kitenbergs, *Dr. phys.,* Associate professor, University of Latvia;
Linas Mazutis, *PhD in Biological Chemistry, Professor, Vilnius University.*

The thesis will be defended at the public session of the Doctoral Committee of Physics, Astronomy, and Materials science, University of Latvia, at 15:00 on September 12, 2025, In the University of Latvia House of Sciences, Jelgavas street 3, as well as remotely.

The thesis is available at the Library of the University of Latvia, Raina boulevard 19.

Chairman of the Doctoral Committee _____/ Uldis Rogulis/
(signature)

Secretary of the Doctoral Committee _____/ Sintija Silina/
(signature)

ISBN 978-9934-36-405-1
ISBN 978-9934-36-406-8 (PDF)

ABSTRACT

Prostate cancer is the second most common cancer in men and the fifth leading cause of cancer-related mortality globally. Its detection is complicated by a high rate of false positives and difficulty differentiating between benign and malignant tumours. These diagnostic challenges are compounded by a substantial increase in mortality if the disease progresses to a metastatic stage. In recent years extracellular vesicles (EVs) have emerged as a promising bio marker for non-invasive disease detection. To improve detection of prostate cancer, a microfluidics device for EV sample preparation was developed consisting of a mixing and magnetic separation module. Using passive zig-zag mixer a mixing index of 0.92 was achieved and validated through optical 2D analysis. Furthermore, the 3D mixing mechanism was investigated using confocal microscopy where complex local vortex formation was observed. Magnetic particle separation efficiency exceeded 98% was achieved following the optimization of magnetic arrangements. The most effective setup utilized an array of N45 magnets configured in a North-South alignment. After integrating both modules on a microfluidics chip, the binding kinetics between EVs and anti-CD9 nanobodies were measured. Based on the binding kinetics, after 10 min the EV capture was saturated and comparable to standard laboratory assays, offering a faster alternative to antibody-based immunomagnetic protocols. Furthermore, this thesis reveals the binding kinetics of EVs to anti-CD9 nanobodies for the first time. This thesis demonstrates the potential of the microfluidic device to enhance clinical diagnostics by offering speed and reducing manual labour without compromising accuracy.

STATEMENTS TO DEFEND

1. Off-stoichiometry thiol-ene polymer (OSTE), combined with cyclic olefin copolymer (COC), enables the fabrication of extracellular vesicle sample preparation devices using photolithography and without a thermal cure step.
2. Three-dimensional confocal microscopy of passive microfluidic mixers provides direct experimental evidence of Dean vortices and secondary flow structures at the microscale-phenomena previously unresolved by conventional two-dimensional optical microscopy.
3. Magnetic particles can be separated with over 98% efficiency in a microfluidic device. Extracellular vesicles bound to nanobody-conjugated magnetic particles have asymptotic binding kinetics reaching saturation within 10 minutes in both the microfluidic device and standard method

CONTENTS

GLOSSARY

Abbreviations

AR	Aspect ratio
COC	Cyclic Olefin Copolymer
DNA	Deoxyribonucleic acid
EVs	Extracellular vesicles
LNCaP	Lymph node carcinoma of the prostate
MP	Magnetic particle
Nb	Nanobodies
OSTE	Off-stoichiometry thiol-ene
PDMS	Polydimethylsiloxane
PMMA	Polymethyl methacrylate
QPCR	Real-time polymerase chain reaction
RMI	Relative mixing index
RNA	Ribonucleic acid
UV	Ultraviolet
WB	Western blot (protein immune blot)

Characteristic quantity

σ	Standard deviation of the pixel intensities
σ_0	Standard deviation of the pixel intensities in the unmixed case
<I>	Average pixel intensities in the cross section
d	Diameter (m)
De	Dean number
I_{oi}	Local pixel intensity in the unmixed state
N	Total number of pixels
r_C	Curvature radius (m)
Re	Reynolds number

INTRODUCTION

The importance of developing a new and improved medical devices cannot be overstated, particularly for diseases like cancer, where early detection is crucial for reducing cancer mortality. However, current detection methods often face limitations related to complexity, cost, accuracy, and practicality, making them less effective for routine use. These challenges are especially evident in the early stages of cancer, where subtle physiological changes make detection difficult with existing methods.

This dissertation addresses these challenges with a focus on prostate cancer. It begins with a literature review of the disease, current detection methods and microfluidics approach to detection. The experimental part addresses the whole device cycle starting form fabrication and ending with bioreactor grown prostate cancer extracellular vesicles (EV) that are tested in microfluids device and compared to standard laboratory methods.

The creation of a microfluidics device requires the combination of concepts from engineering, physics, and biology, forming the foundation of microfluidics a field that precisely manipulates small volumes of liquids, starting from picolitres in droplet microfluidics up to microliters for diagnostics and biosensing, to enhance functionality and process efficiency. This is largely due to the unique physical phenomena that occur at small scale, such as the increased importance of capillary forces, the predominance of laminar flow, and the drastic increase in surface-to-volume ratio. Additionally, the reduction in required reagent volumes lowers costs, and complex biological processes can be simplified due to the smaller scale and reduced interactions.

Whiles microfluidic devices can improve the detected efficacy they cannot exceed biological limitations of currently used markers such as prostate-specific antigen testing which suffer from high false-positive rates. To improve biological markers EV can be used, which starting from 2014 were acknowledged as messenger molecules. EVs are a closed bilipid layer structures that contain messenger molecules such as ribonucleic acid (RNA) and proteins, which are released by all cell types and can influence cellular processes. An analogy can be drawn to WhatsApp messages where a message can make you go make a cup of tea instead of coffee. EVs are even more interesting in that healthy cell and cancer cell released EVs can be differentiated thus serving as an early indicator.

By combining the advantages of microfluidics with the potential of EVs as early cancer markers, this work aims to advance the development of a novel detection device that offers a meaningful improvement over current method.

Research aim

Further the development of microfluids device made of thermoplastics and to investigation of the microfluidics device applicability for prostate cancer detection via liquid biopsy using extracellular vesicles.

Research objectives

- Develop fabrication process for a microfluids device that is superior to polydimethylsiloxane fabrication process in terms of scalability and small molecule absorption.
- Create a quality control procedure for the fabrication process.
- Develop mixing and magnetic separation module as sample preparation for downstream analysis.
- Quantify the mixing modules using 2D and 3D visualization methods, thus finding the optimal design based on relative mixing index.
- Quantify the performance of the magnetic separation module and optimize the design to acquire 95%+ capture efficacy.
- Evaluate the combined system of magnetic particles (MP) and bioreactor grown EVs in microfluids device and compare it to standard system.

Scientific novelty

The scientific novelty lies in the advancement of microfluidics for prostate cancer detection through enhanced EV extraction techniques and the integration of microfluidic modules.

- **Fabrication Process**. This thesis shows the fabrication for off-stoichiometry thiol-ene (OSTE) and cyclic olefin copolymer (COC) device (OSTE-COC) using reaction injection moulding using OSTE220 polymer. This method, to the best of the author's knowledge, has not yet been applied in device fabrication for prostate cancer sample preparation. This approach offers advantages over previous methods used in organs-on-chip[1] and EV separation[2] applications.
- **Flow Pattern Visualization**. Detailed 3D confocal images of the flow patterns, as presented in the thesis, are rarely found in scientific literature. These images contribute to the understanding of fluid dynamics, particularly in the areas of Dean vortices and secondary flow.
- **EV Capture Antibodies**. novel anti-CD9 nanobodies were used for EV capture instead of conventional antibodies, considerably increasing capture efficacy and reducing nonspecific binding.
- **Device Integration and Potential**. The final device, due to its fabrication and ability to integrate multiple modules, shows promise for further development and potential clinical adoption.

- **Kinetic Profile of EV-MP Binding**. The kinetic profile of EV and MP binding using CD9 nanobodies, as characterized in this study, has not been previously reported, providing valuable information for similar systems.

Practical significance

Research in prostate cancer detection is considered to hold considerable potential for reducing mortality rates, as the likelihood of successful treatment is dramatically increased by early detection [3]. Given the relatively recent discovery of EVs as biomarkers secreted by all cell types, the development of EV-based assays is viewed as a pathway for comprehensive testing solutions [4]. Moreover, advancements in microfluidic devices within the diagnostics field could lead to substantial cost reductions and improved convenience, ultimately enhancing healthcare outcomes [5]. This research represents a step in transitioning microfluidic devices from laboratory settings to practical applications, by providing a fabrication protocol for small to medium-scale production, facilitating rapid prototyping and real-world testing. Lastly, the fundamental insights gained from 3D flow visualisation and kinetic profiling contribute to the broader scientific understanding in this field.

Author's contribution

The author fabricated and characterized the microfluidic device. This involved designing the device, adapting the fabrication process from existing literature, optimizing key parameters, and conducting quality control. The development of fabrication protocol for the microfluidic device was supported by Roberts Rimsa, Arnita Spule, Gunita Paidere, and Karlis Grindulis, who contributed through shared insights, tips, and collaborative efforts in similar processes.

The author independently conducted the optical 2D mixing experiments, while the 3D visualization experiments were performed with the assistance of Feliks Rumnieks, who operated the microscope.

The testing of the microfluidic device using biological samples was a collaborative effort with Latvian biomedical research and study centre, specifically with Edgars Endzelins. The author provided fabricated microfluids devices, developed flow control sequences, operated the microfluidics system and set up experiments from the microfluidics perspective. The final experimental setups were developed in cooperation with Edgars Endzelins.

Western blotting, real-time polymerase chain reaction (qPCR), and iron content measurements were performed by Edgars Endzelins, while the data analysis was conducted by the author, with support from Edgars Endzelins.

List of publications

Publications included in this Thesis

1. J. Cipa et al., "OSTE DEVICE FOR MAGNETIC PARTICLE CAPTURE," MicroTAS 2022 – 26th International Conference on Miniaturized Systems for Chemistry and Life Sciences, pp. 919–920, Jan. 2022.
2. J. Cipa, E. Endzelins, A. Abols, N. Romanchikova, A. Line, G. W. Jenster, G. Mozolevskis, R. Rimsa. "Elucidating Extracellular Vesicle Isolation Kinetics via an Integrated Off-Stoichiometry Thiol-Ene and Cyclic Olefin Copolymer Microfluidic Device". Polymers 2024, 16, 3579. https://doi.org/10.3390/polym16243579

Publications not included in this thesis or previous qualification work.

1. B. Berzina et al., "Luminescence of AlN:Eu ceramics: Properties and mechanisms," *Opt Mater (Amst)*, vol. 127, p. 112217, May 2022, doi: 10.1016/j.optmat.2022.112217.
2. A. Antuzevics et al., "Thermal properties of paramagnetic radiation-induced defects in lithium orthosilicate containing breeder material," *Journal of Nuclear Materials*, vol. 565, p. 153713, Jul. 2022, doi: 10.1016/j.jnucmat.2022.153713.
3. R. Ruska et al., "Off-Stoichiometry Thiol-Ene Surface Functionalization: Example with Gold Nanoparticles" *Materials* 2024, 17(24), 6135; doi: 10.3390/ma17246135

List of international conference presentation about thesis

1. Janis Cipa, Roberts Rimsa, Gatis Mozolevskis, "MICROFLUDIC MIXERS AND MAGNETIC PARTICLE CAPTURE CHAMBERS BASED ON OSTE POLYMER", *80th International Scientific Conference of the University of Latvia, Riga Latvia, 2022*
2. Janis Cipa, Edgars Endzelins, Roberts Rimsa, Artis Galvanovskis, Arturs Abols, Aija Line and Gatis Mozolevskis, "OSTE DEVICE FOR MAGNETIC PARTICLE CAPTURE," *MicroTAS 2022 – 26th International Conference on Miniaturized Systems for Chemistry and Life Sciences, pp. 919–920, Jan. 2022.*
3. Janis Cipa, Roberts Rimsa, Gatis Mozolevskis, "Fabrication of passive microfluidics mixing device based on Off-stoichiometric thiol-ene and Cyclic olefin copolymer", *39th Scientific Conference of the Institute of Solid State Physics, University of Latvia, 28 february to 2 march, 2023.*

4. Janis Cipa, Felikss Rumnieks Roberts Rimsa, Aija Line, Gatis Mozolevskis "Gravity effects in zig-zag microfluidic mixers for light dye molecules?" *SMILS 2023, Stockholm, May 30–31, 2023*
5. Janis Cipa, Edgars Endzelins, Roberts Rimsa, Arturs Abols, Aija Line and Gatis Mozolevskis, "Polydimethylsiloxane-free microfluidic technology for the rapid capture of extracellular vesicles from urine" *MicroTAS 2023, Katowice, Poland October 15–19, 2023*
6. Janis Cipa, Edgars Endzelins, Roberts Rimsa, Arturs Abols, Aija Line and Gatis Mozolevskis. "Enhanced isolation of cancer-derived extracellular vesicles using PDMS-free microfluidic device" *40th Scientific Conference of the Institute of Solid State Physics, University of Latvia, March 5–7, 2024.*

1. LITERATURE OVERVIEW

Over the past decade, EVs have been recognized as key biomarkers for the detection of complex diseases, including cancer, neurodegenerative, and cardiovascular diseases. [6] EVs are heterogeneous, membrane-bound vesicles secreted by almost all cell types, carrying various messenger molecules that can trigger different cellular responses. EV analysis has the potential for improved disease detection, especially in the case of liquid biopsy, which could be used to detect disease, monitor disease progression, and determine drug efficacy, with the goal of improving patient care. [7, 8] However, the implementation of EV-based diagnostics in clinical settings has been hindered by the lack of robust, efficient, and reproducible methods for isolating specific EV subpopulations. This challenge is further complicated by their broad size distribution, ranging from 30 nm to 2000 nm, which creates difficulties for standard laboratory assays. [6]

Several methods, such as ultracentrifugation [9], size exclusion chromatography [10], precipitation, [11] and others [12] have been employed for the separation and analysis of EVs. Despite these approaches, the challenge remains to isolate specific EV subpopulations that are free from cell debris and non-specific EVs as well as to enrich EVs for quantitative downstream analysis. Immunomagnetic isolation has emerged as the gold standard due to its efficiency, speed, scalability, and specificity in extracting EVs. [13–19] This method has been applied in various fields, including bacterial capture and DNA extraction [20], metabolite capture [21], EV separation [9], and others [22].

Building on typical laboratory techniques, microfluidic devices have shown considerable potential in EV separation. Microfluidics devices have demonstrated better enrichment compared to traditional methods like ultracentrifugation [9], alongside higher throughput [23], reduced sample volume [24] and decreased labour intensity. Notably, Wang et al. demonstrated the efficiency of a microfluidic device using magnetic particles and Raman spectroscopy, which successfully distinguished between cancer patients and healthy individuals within an hour, achieving an EV capture efficiency of 72.5% [25]. However, a limitation of current EV-separation devices is the slow flow rate of 0.3 μl/min, which, for a typical clinical sample of at least 100 μl, would take 5.5 hours to meet the standard limit of detection [26].

Despite the advantages of microfluidic devices, their widespread application in EV diagnostics has been restricted by the materials typically used in their fabrication. Polydimethylsiloxane (PDMS), commonly used in prototyping microfluidic devices, poses challenges for mass production and tends to absorb lipophilic molecules [27, 28], limiting its effectiveness in EV analysis. Moreover,

in biological sample applications, the need for sterility necessitates single-use devices, rendering PDMS economically impractical due to high costs.

To address these limitations, alternative polymers such as thermoplastics are actively being explored. Promising candidates include cyclic olefin copolymer (COC) and off-stoichiometry thiol-ene polymer (OSTE), both of which show potential in reducing hydrophobic molecule absorption and offering fabrication versatility [28–31]. COC has been widely used as a biocompatible and transparent thermoplastic in various microfluidic applications, [32] while OSTE materials have been used for applications such as synthetic paper, [33] spider silk fabrication, [34] and as channels for photonic biosensors. [35] Yet to the best of authors knowledge, OSTE-COC devices have only been fabricated for organs on chip [1] and flow field-flow fractionation EV separation [2] applications rather than microfluidic EV-sample preparation tool or for immunomagnetic separation.

To advance EV extraction techniques and further integrate microfluidic biosensing applications, this thesis adopts a comprehensive approach, covering the entire workflow from device fabrication to biological application. A proof-of-principle EV extraction device is introduced, which integrates mixing and magnetic particle capture functions on a PDMS-free chip. The proposed system not only improves the scalability of EV extraction but also offers a practical and versatile platform for testing liquid biopsy samples containing EVs, paving the way for future clinical applications.

2. FABRICATION

To create a microfluidics device for prostate cancer detection using EVs sample must first be prepared for downstream analysis. In the case of immunomagnetic capture sample must be mixed with MPs coated with antibodies or nanobodies and then subsequently separated out of the flow thus only EVs of interest remain. This leads to the requirement of 2 separate modules, first to mix the MPs and EVs and second to elude captured EVs on MPs using magnetic force.

2.1. Desing and 3D printing

Device fabrication starts with designing a microfluidic device using computer assisted design (CAD) program. A typical device design consisted of three core components: fluid connectors such as mini luer, COC slide for device top and bottom serving as a transparent layer and OSTE layer in between forming the channel side walls (Figure 1).

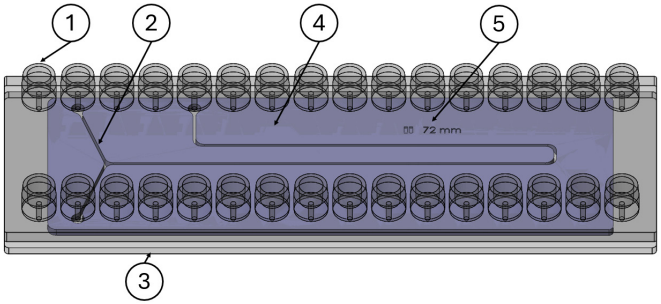

Figure 1. Microfluidics device made of COC microscopy slide with mini luer connectors (1), 200 μm × 200 μm channel (2), COC microscopy slide (3), OSTE layer (4), and a reference marker (5).

The microfluidic device was then fabricated following soft lithography methods, where a double negative mould was 3D printed using Zortrax Inkspire 3D printer, with a pixel size of 50 μm and a layer height of 50 μm. An ivory-white resin was used, with Young's modulus of 2 GPa and a volumetric shrinkage rate of 4%. For soft lithography moulds, Sorta clear™ silicone was used instead of SYLGARD 184 due to its reduced adhesion to OSTE. As an initial application, a device for magnetic particle separation was designed and fabricated.

2.2. OSTE 322 reaction injection moulding

Magnetic particle separation devices were fabricated using OSTE, a thermoplastic polymer that has a two-step curing process. The process begins with filling of OSTE 322 into flexible polymer mould based on magnetic capture chamber design. After which OSTE 322 was illuminated with UV light to induce polymerization, converting the material from liquid to a tacky solid capable of covalently bonding to COC substrates (Figure 2). This facilitates the creation of OSTE-based channels and allowed subsequent device sealing using a COC slide with microfluidic compatible ports such as mini-luer. After which device was thermally cured to complete the polymerization and create a permanently sealed device. This process flow is called OSTE reaction injection moulding (OSTE-RIM) and it does not require high pressure or extensive thermal management. As a result, the mould can be made using standard soft lithography or alternatively metal mould can be formed, considerably reducing costs compared to traditional injection moulding thus enabling rapid prototyping. [36]

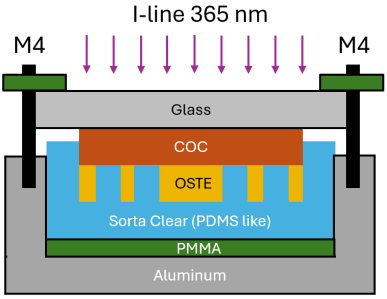

Figure 2. Side view schematic of reaction injection moulding stack for OSTE322 (not in scale).

In this way, microfluidic devices with different magnetic capture designs were efficiently fabricated, converting capillary or bulk-based magnetic capture into compact, chip-based platforms that support automation and compatibility with additional microfluidic modules (Figure 3).

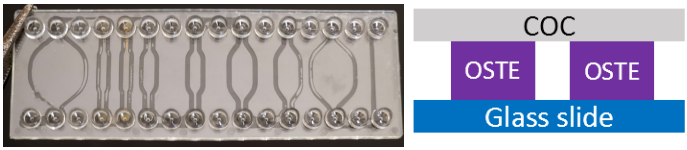

Figure 3. Finished OSTE 322 device on the left and the side view of the device on the right.

2.3. OSTE 220 reaction injection moulding

Limitations were encountered when applying the OSTE 322 fabrication method to micromixer devices. The achievable resolution was restricted to the range of several hundred micrometres, which prevented the formation of sharp corners. Additionally, the moulding process does not allow for the integration of internal channel structures, which can enhance mixing efficiency. To address these limitations, an alternative fabrication method was developed, drawing on the OSTE 220-based protocol. Although the OSTE-RIM process has been previously described by N. Sandström [36], in this work it was adapted to fabricate a hermetically sealed OSTE-COC composite device.

A modified process was implemented to improve resolution and eliminate the need for a thermal curing step. This approach, based on the protocol outlined in Section 3.2, employed OSTE 220 as a negative photoresist. Microstructures were defined by selectively exposing the OSTE layer to UV light through a photomask, inducing polymerisation in the exposed regions. This enabled the formation of features with a minimum size of few micrometres. Achieving such resolution was necessary, as mixing in laminar flow conditions can be enhanced using sharp channel features to promote local vortex formation. [37]

For the moulding step, QSil 216 (CHT) silicone was used in place of Sorta Clear. QSil 216 is a PDMS-like material that combines the handling characteristics of SYLGARD 184 with reduced adhesion to OSTE, improving the demoulding process. COC slides were used as the base substrate instead of glass, due to improved adhesion with OSTE. Given the relatively low UV dose required to polymerise OSTE 220 (approximately 100 mJ/cm^2), a PMMA spacer was incorporated to reduce UV reflection and prevent unintended curing. The device height was defined by the mould, while compression during assembly was controlled using six screws, each tightened with a torque wrench set to 0.3 Nm. The mould was filled with OSTE 220 and exposed to UV light through an I-line filter at a final dose of 50 mJ/cm^2 (Figure 4).

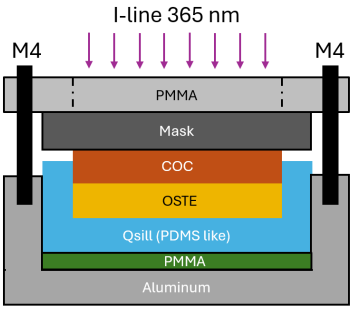

Figure 4. OSTE 220 reaction injection moulding jig side view schematic (not in scale), where dash dot lines represent a cut, and mask is not covered by PMMA plate.

Post exposure the COC slide with OSTE layer was developed in acetone using an ultrasonic bath, followed by isopropanol rinsing, N_2 drying, and post-bake at 60 °C. Prior to bonding, an O_2 plasma treatment was applied to the COC slide with mini-luer connectors. The layers were aligned, clamped, and UV-exposed (4000 mJ/cm^2), resulting in a hermetically sealed device with a burst point exceeding 400 µl/min (Figure 5).

This device offers excellent optical transparency and high-pressure tolerance, while also allowing for the use of standard mini Luer connectors. Furthermore, the fabrication protocol builds on our previous work at Micro and Nanodevices Laboratory by decreasing feature size down to 20 µm and improving fabrication speed as this fabrication method allows to remove thermal treatment, thus the ready device can be made in under one hour in laboratory setting [30]

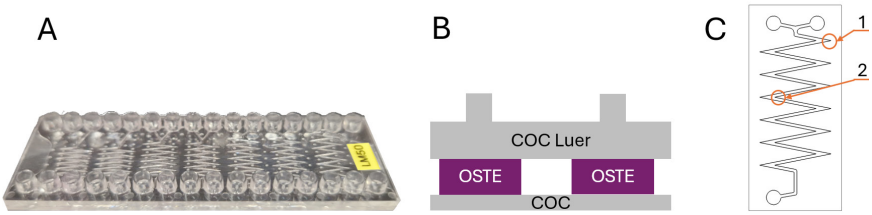

Figure 5. Microfluidic mixing device (A), side view of the device (B), and schematic view (C) where 1 is outer corner and 2 is inner corner.

3. RESULTS AND DISCUSSION

3.1. Performance Assessment of a passive microfluidic mixer

The performance of the mixing device was assessed using aqueous solution of Rhodamine B, and de-ionised water. By infusing aqueous solution of Rhodamine B and water in a single channel and maintaining a constant flow, optical measurements were performed at the end of the channel as shown in Figure 6. the mixing efficiency of the device was determined by using relative mixing index (1) similarly to other microfluidics works [38, 39].

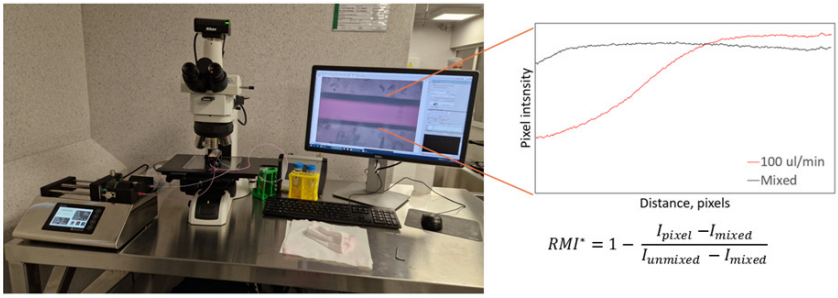

Figure 6. Photograph of mixing setup on the left and mixing data example on the right, where x axis is the channel width. All values are integrated across channel length, and mixing value are taken at a constant flow rate whereas mixed value is after flow has stopped for 5 minutes.

To mathematically quantify mixing of 2 liquids relative mixing index was used which is described by equation (1) [40]:

$$RMI = \frac{\sigma}{\sigma_0} = \frac{\sqrt{\frac{1}{N}\sum_{i=1}^{N}(I_i - \langle I \rangle)^2}}{\sqrt{\frac{1}{N}\sum_{i=1}^{N}(I_{oi} - \langle I \rangle)^2}} \quad (1)$$

Where, σ – standard deviation of the pixel intensities, I_i – local pixel intensity, <I> or I_{mixed} – average pixel, intensities in the cross-section, N – total number of pixels, σ_0 – standard deviation of the pixel intensities in the unmixed case, I_{oi} – local pixel intensity in the unmixed state.

While mixing index is strictly defined, mixing efficiency noted in percentage is rather inconsistent across literature, yet in most cases a conversion from index to percentage can be made. For the fabricated microfluidics device relative mixing

index of 0.92 was achieved using a design with 12 sharp corners and a total channel length of 70 mm. The achieved mixing performance is comparable to literature results, where a mixing index of 0.96 was achieved in a 77 mm long, staggered, curved channel [41]. Although designs like the herringbone mixer offer a higher mixing performance by utilizing grooves to enhance mixing over a shorter distance, [42] these designs present the drawback of potentially trapping EVs within the grooves. Furthermore, the developed planar passive zigzag mixer demonstrates comparable performance to other reported designs and can be easily extended for improved mixing, owing to its modular nature.

To validate the acquired mixing values a data set of 54 points were evaluated using ANOVA test. Where bottom diagonal represents Pearson coefficient, and above diagonal shows the p values. The Pearson correlation coefficient quantifies the strength and direction of the linear relationship between two variables. It ranges from –1 to 1, where a value of 1 indicates a perfect positive correlation, –1 denotes a perfect negative correlation, and 0 signifies no correlation. The correlation matrix (Figure 7) demonstrates a strong relationship between increased flow rate and improved mixing efficiency ($r = 0.67$) that is significant ($p = 2.57 \times 10^{-8}$), indicating that higher speeds in a passive micromixer led to better mixing. Additionally, reducing the channel size from 300 µm to 200 µm resulted in a statistically significant ($p = 9 \times 10^{-5}$) improvement in the relative mixing index ($r = -0.51$), likely due to enhanced local chaotic flow, including Dean vortices and secondary flow generated at the mixer's sharp bends. [43] Interestingly, no significant impact was observed for bend angle from 22.5 to 14 degrees ($r = 0.04$, $p = 0.278$), with the analysis performed at a 95% confidence interval, which aligns with findings from Cosentino et al. [44]

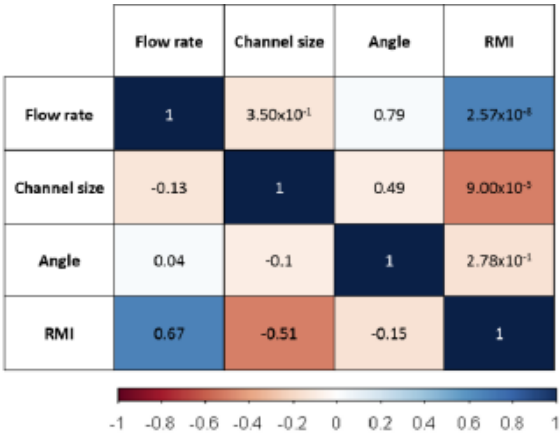

Figure 7. The correlation matrix of relative mixing index for mixing devices, calculated by Pearson correlation coefficient, where above middle diagonal represents p-value of the correlation coefficient.

Nevertheless, these results stem from the assumption that 2D optical microscopy can be used to fully determine mixing process for a microfluids device. The issue with this assumption is that channels have depth and non-ideally straight walls due to the fabrication process, this leads to potential 3D effects which are missed.

3.2. 3D effects in mixing

While the majority of mixing designs are evaluated using brightfield or fluorescence microscopy, these methods primarily assess the flow at the top layer of the device, missing important details in the bulk of the flow. To gain deeper insights into the processes occurring within the mixer, confocal fluorescence microscopy was employed. This technique enables 3D scanning of the flow, leveraging the laminar nature of the system. Since laminar flow is independent of time, formed vortices can be observed, as they are not transient phenomena.

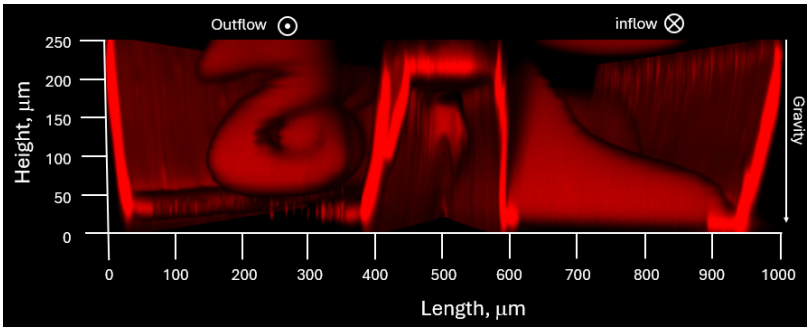

Figure 8. Confocal microscope image of rhodamine B and deionised water mixing at the first sharp bend of zig-zag mixer.

As shown in Figure 8, each corner of the device facilitated the formation of a vortex, increasing the diffusion area and enhancing mixing efficiency. This phenomenon, known as secondary flow from which Dean vortices form, occurs when a flow encounters a corner where, due to inertial effects, U-shaped flow profile is created. U-shaped profile was experimentally validated by a single channel with 1000 µm radius curve as show in Figure 9.

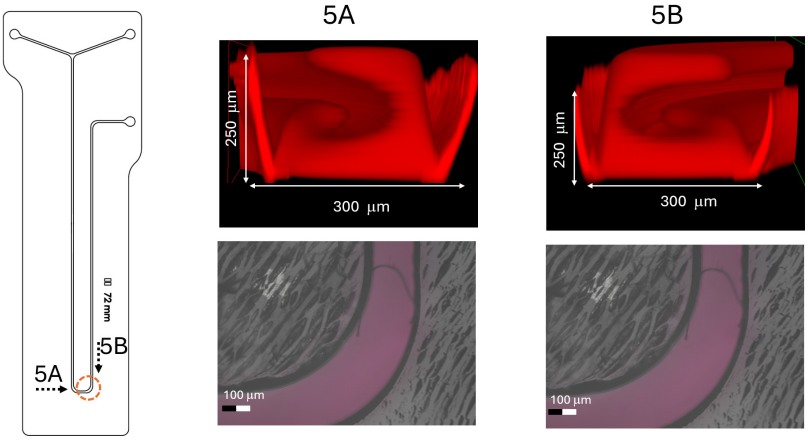

Figure 9. Confocal and optical microscopy image at 2nd bend looking from inlet 5A and outlet 5B indicated by the doted arrow.

Secondary flows and Dean vortices are the basis of the mixing process in passive mixing designs. The intensity of this process can be described by a dimensionless quantity called the Dean number. Dean's number (*De*) is mathematically described by the equation:

$$De = Re\sqrt{\frac{d}{2r_c}} \quad (2)$$

Where *Re* – Reinhold number, *d* – channel diameter (for a round channel), r_c – radius of the curvature. The developed zig-zag passive mixing device has a Dean number of 33.3. However, this value is too small to fully explain the intensity of the observed vortices. [45] One possible explanation is that the channel walls were not perfectly straight and had defects such as holes and ridges that contributed to the formation of vortices. Nevertheless, this improves the overall understanding of the mixing module thus, it should be considered in case of further optimization.

3.3. Magnetic separation

Having established the efficacy of dye-based methods for evaluating the mixing dynamics within microfluidic channels, we now turn our focus to the subsequent phase of project–magnetic capture and device optimisation. To test the magnetic capture efficiency OSTE 322 devices with different aspect ratio MP separation chambers were tested. For the testing, iron core microparticles were flown through the chamber with a magnet positioned underneath. Both

the outflow and captured particle were collected, dissolved in *Aqua regia*, and then the iron content was quantified via optical absorption.

To assess the limitations of magnetic particle capture efficacy in the microfluidic system, several magnetic configurations were evaluated. Initial tests using a single N52 permanent magnet yielded a particle capture rate of less than 60% for a channel width of 2 mm and height of 0.5 mm. To improve this performance, multiple alternative setups were tested and compared against the original design (Figure 10a):

- **Dual Magnet Setup**: A configuration with two N52 magnets, positioned above and below the channel. Figure 10b.
- **Magnet Arrays using:** 18 N45 magnets stacked laterally in opposing polarity. Figure 10c.
- **Magnet Arrays using:** 18 N45 magnets stacked in Halbach array, Figure 10d.

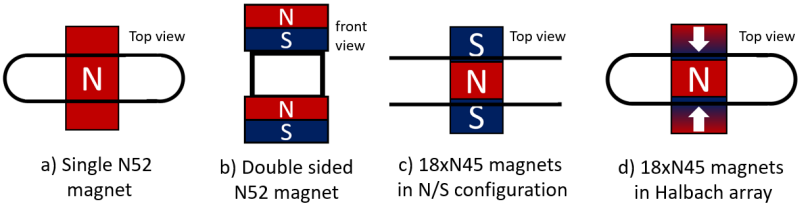

Figure 10. Schematic of different magnetic configurations for the microfluidics device.

Central to the effectiveness of magnet configurations is the generation of a non-uniform magnetic field. This non-uniformity causes particles passing through the magnetic field gradient to experience higher forces, facilitating their capture at the bottom of the device. The effect is particularly pronounced in the Halbach array, where the magnetic field is directed from bottom to top, considerably increasing magnetic field strength compared to the simpler north/south (N/S) configuration, in which the field strength is distributed equally on both sides. By comparing different setups as seen in Figure 11, particle capture efficiency of over 98% was achieved. Among the tested configurations, the Halbach array had marginally better performance. However, due to the complexities involved in its fabrication and inherent instability, (N/S) configuration was chosen for subsequent experiments.

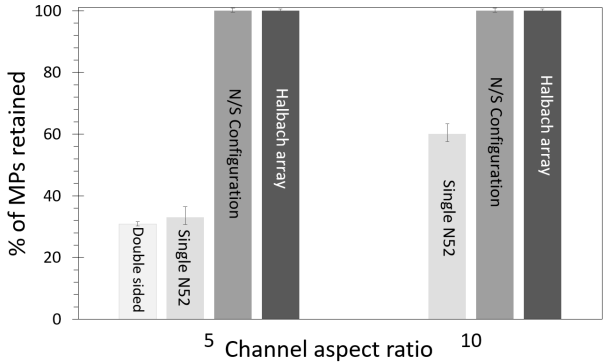

Figure 11. MP retention based on different magnetic configurations

3.4. Particle separation using biological sample

To ensure the viability of EVs in microfluidic systems, their stability was assessed. This evaluation was necessary because EVs are fragile, and high shear stresses induced by secondary flow can disrupt their membranes, leading to the release of EV cargo and rendering them ineffective. To determine whether membrane disruption occurred due to shear forces induced by the channel walls, laminar flow profile, or other factors, EV durability was assessed as a function of flow rate by examining EV content using the qPCR method (Figure 12A). A notable observation was that the reference EV sample that was stored at +4C degraded over time as seen in Figure 12B, thus a linear correction was applied to the data set to account for lost EVs.

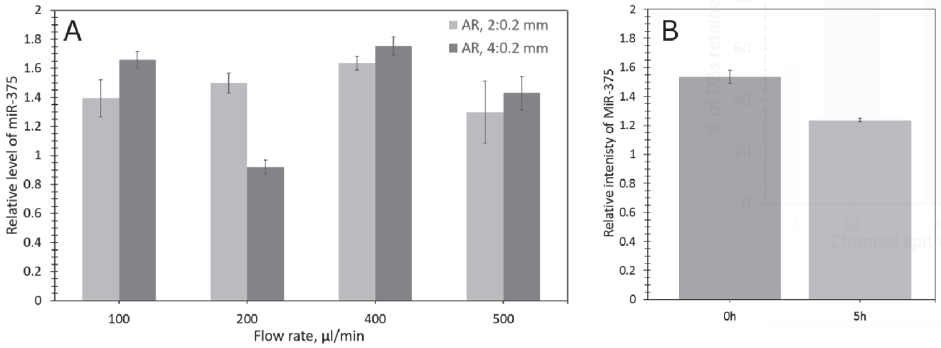

Figure 12. QPCR of miR375 protein extracted from captured EVs based on flow rate (A), and reference EVs stored at +4 °C (B)

qPCR data, as shown in Figure 12A indicates the presence of micro ribonucleic acid (miR-375), which is prostate-specific and would only be detected if encapsulated within EVs. This is because any stray ribonucleic acid (RNA) is rapidly degraded by ribonuclease, which is ubiquitous. The primary takeaway from this graph is that RNA can successfully be detected from EVs captured within the microfluidic device. Furthermore, it was observed that for flow rates ranging from 100 to 500 µL/min, there was negligible difference in EV integrity between conditions, indicating that EVs remained intact under this flow rate range, corresponding to a shear stress of 1.4 Pa.

3.5. Integration of modules

To improve the interaction of biological samples within the microfluidic device, the channel length was increased from 74 mm to 800 mm, and the number of channel bends was increased from 12 to 510. A 140 µm-thick COC film was used in place of the previous 1000 µm rigid COC slide, which enhanced bonding efficiency and overall device yield. In contrast to earlier designs that incorporated multiple independent channels, the updated layout features a single continuous channel covering the entire slide. This modification increased fabrication sensitivity and required higher precision during processing.

To compensate for mould shrinkage and the flexibility of the thinner film, a shrinkage correction factor of 0.67% was applied. Device exposure and development parameters were optimised with a final dose of 107.5 mJ UV light and 75 seconds in acetone, resulting in reproducible formation of microfluidic channels with final dimensions of 200 µm × 200 µm × 800 mm. Additionally, an integrated magnetic separation module (4 mm × 200 µm × 18 mm) was incorporated into the same device (Figure 13).

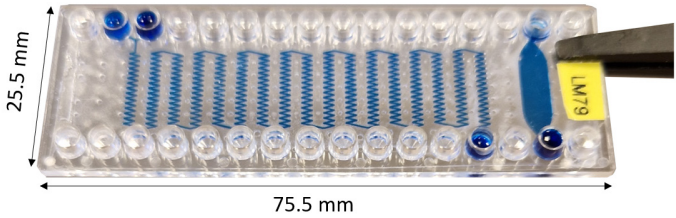

Figure 13. Integrated mixing and magnetic capture device on a single COC slide

3.6. Quality control

To increase production scale and create device suitable for biological sample analysis additional quality control had to be introduced. As biological samples will have to use different devices to ensure sterility, all fabricated devices must be as similar as possible. Thus, height measurements were performed across the whole device to evaluate the device quality as indicated in figure 14.

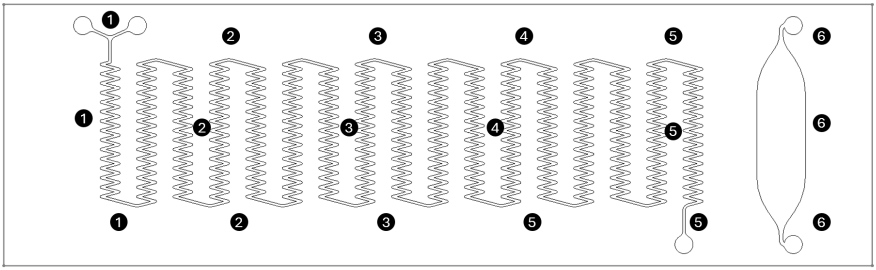

Figure 14. Measurement points on the device, the number indicates the columns that were measured.

An important aspect of device characterisation involved determining the height of the OSTE layer. Two measurement approaches were evaluated: an optical microscopy-based method and a micrometer-based method. In the optical method, the device height was estimated by sequentially focusing on the top and bottom surfaces and calculating the difference in focal planes. In contrast, the micrometer-based method involved measuring the total thickness using a digital micrometer, then subtracting the known thickness of the substrate to obtain the thickness of the OSTE layer. A comparison of the two methods is shown in Figure 15.

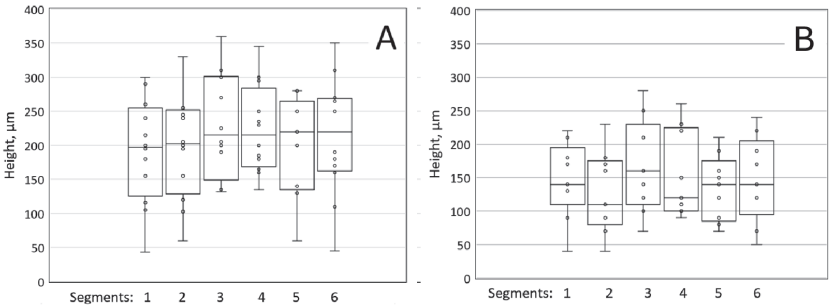

Figure 15. Optical microscope (A) and digital micrometre (B) height measurements of columns, where each box and whiskers represent a different segment of 4 devices, as noted in Figure 14.

The results indicated only minor differences between the two measurement techniques. However, there was slightly higher variability for the optical method, likely due to difficulties in consistently achieving precise focus at each measurement point directly influencing the height measurement. Owing to its lower variability and faster operation, the micrometer-based method was selected for subsequent measurements.

3.7. Device integration testing

To successfully combine mixing and magnetic separation modules, it was necessary to test them with a biologically similar sample to prostate cancer and compare microfluidic device results with a standard method. For this purpose, the extracellular vesicles of prostate cancer grown in the bioreactor prepared by Latvian Biomedicine and Study centre were used.

To test the microfluidic device, a semi-automated sample handling sequence was developed, which included sample mixing, capture, and washing. This automated approach was compared to the standard method for EV capture. The semi-automated system relied on preloaded syringes in a syringe pump, while the standard method involved over 10 manual steps, including multiple pipetting and particle resuspension steps.

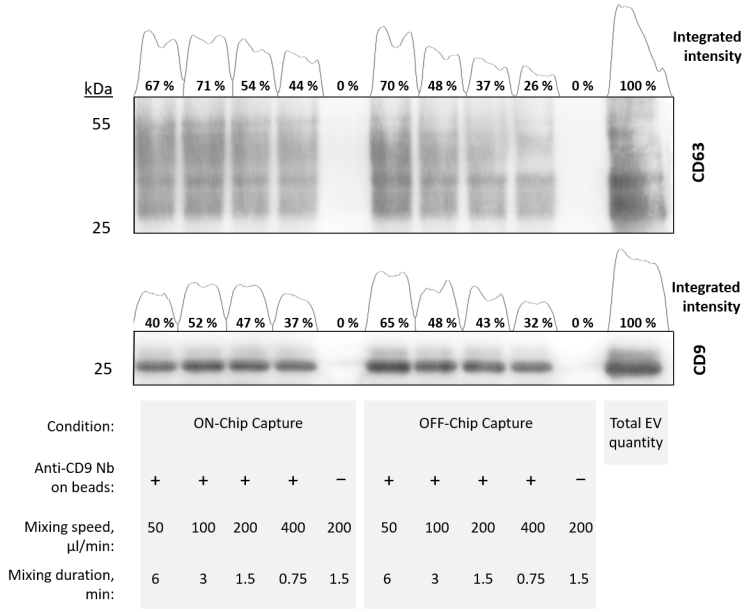

Figure 16. EV survivability based on flow rate and capture type, for integrated system. The top image is Western blot gel, where darker band indicates higher intensity, which is represented by integrated value above.

In Figure 16 EV survivability based on flow rate and capture type for the integrated and non-integrated system is shown. The top of Figure 15 is an image of a Western blot (WB), where the darker the band, the higher the concentration, which is represented by the integrated values above each band. The Figure distinguishes experimental conditions with and without magnetic particles functionalized with surface proteins, specifically CD9 nanobodies that target CD9 proteins on EVs. The experiments using unfunctionalized (–) magnetic particles demonstrated minimal non-specific binding (below 0.5%), confirming that the interaction between EVs and magnetic particles is CD9-specific.

A notable observation was that off-chip capture (the standard method) yielded higher signal intensity compared to on-chip capture (the microfluidics setup). This discrepancy is likely due to the differing setups: the microfluidics system captures EVs on-chip, ensuring that non-captured EVs are immediately removed, while the standard method allows for post-mixing interaction in the container, providing a longer incubation period and enhancing the overall signal intensity. As a result, while the microfluidics system provides a more precise and controlled interaction, the signal intensity is slightly lower due to the shorter incubation time.

At 45 seconds, a potential drop in intensity was observed, which could indicate either a measurement error or the beginning of EV integrity loss. However, this remains speculative without more concrete evidence, as the WB data lacks well-defined error bars. Additional experiments with multiple repeats would be necessary to validate this hypothesis. Nevertheless, to minimize the likelihood of EV membrane disruption in further experiments, the flow rate was reduced to maintain a wall shear stress below 5 Pa.

To further enhance binding efficiency and gain a better understanding of the binding process, the system was adjusted to allow multiple cycles through the mixer. This increased the interaction time between EVs and MPs, providing better binding efficiency and clearer insights into the dynamics of the EV-MP interactions.

3.8. Analysis of integrated device with EV sample

From Figure 16, it can be seen that after mixing, less than 60% of the total EVs were captured in the microfluidic device, which could indicated insufficient mixing. Although the optimization performed based on the dye assays would guarantee 99% mixing after no more than 30 turns, the 60% obtained confirms a considerable difference between the dye assay and the enzymatic reaction case, as that of MPs and EVs. To solve this problem, repeated mixing or recirculating of the sample was introduced. Recirculating refers to flowing the liquid sample through the mixer, storing it in tubing, and then reversing the flow back through

the mixer at the same speed. This process was repeated multiple times, as indicated by the incubation times, ranging from 5 to 50 minutes (1–10 cycles). The test was conducted in parallel with a standard laboratory setup that used a tabletop mixer, magnetic stand, and multiple pipetting steps. In contrast, the microfluidics system was operated semi-automatically, with preloaded samples and washing liquids, reducing manual intervention to the removal of the magnet for elution of the EVs and MPs from the device. Both microfluidics and standard lab protocols ended with sample lyses and sample analysis using WB, as shown in Figure 17.

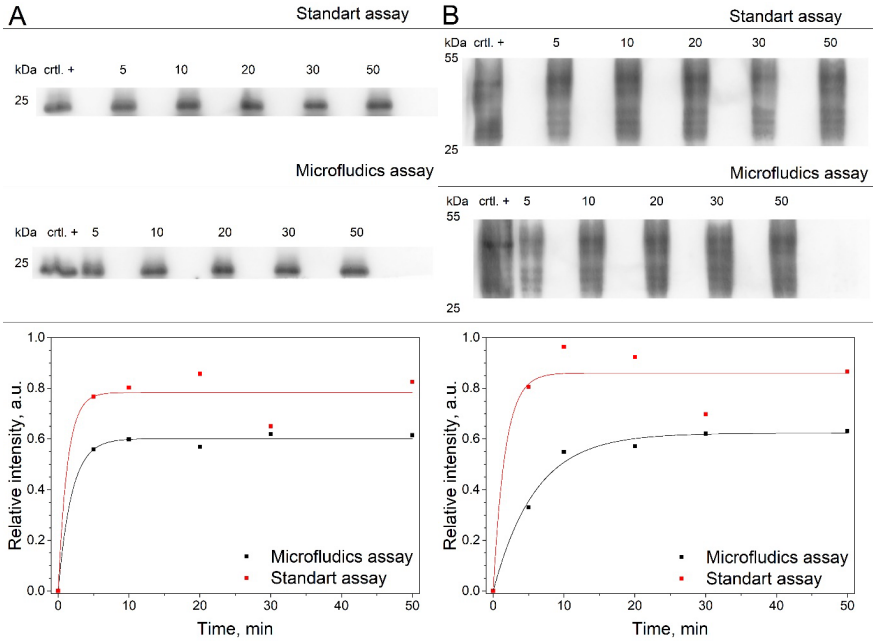

Figure 17. WB analysis showing the efficiency of EV capture. Anti-CD9 nanobody capture and CD9 detection (A) and WB results for anti-CD9 nanobody capture and CD63 detection (B) and each data point is an integrated value relative to total EV quantity. The top figure is WB gel image which is the basis for data.

Figure 17A shows the WB images of CD9 capture and CD9 detection whiles Figure 17B shows CD9 capture and CD63 detection. The relative intensity stems from a control sample where no experimental manipulation was performed and correspond to same EV concentration (crtl. +).

The WB signal in Figure 17A demonstrates that the maximum relative binding efficiency of EVs to MPs is $f_{\infty} = 0.60 \pm 0.01$, which is comparable to

the standard laboratory assay value of $f_\infty = 0.78 \pm 0.04$. Additionally, the CD63 analysis, using an anti-CD63 antibody as shown in Figure 17B, confirmed the successful capture of EVs or double-positive membrane fragments, rather than free-floating CD9 protein. The consistency of data from both markers supports that the majority of the signal originates from captured double-positive vesicles, with minimal to no contribution from free-floating CD9 protein.

To further evaluate the data an exponential growth model $f = f_\infty\ [1\ -exp(-\sigma t)]$ was fitted for the background corrected integrated WB values using the least square method where a similar model was employed by Petkovica et al. [46]. Here the f_∞ is the asymptotic value of the binding efficiency and σ is the binding, with results summarized in Table 1.

Table 1. asymptotic value of the binding efficiency and the binding rate of integrated WB signals.

	R^2	f_∞	σ
CD9 microfluidics	0.99	0.60	0.53
CD9 Standard assay	0.94	0.78	0.77
CD63 microfluidics	0.99	0.62	0.17
CD63 Standard assay	0.92	0.86	0.60

The data reveals that the majority of EV binding to MPs occurs rapidly, within the first 10 minutes of the reaction as shown in Figure 17. This marks a considerable improvement compared to conventional laboratory assays, where MP binding to antibodies typically requires one to 24 hours, as reported in multiple MP protocols [47, 48]. The faster binding facilitated by the use of nanobodies instead of antibodies combined with on-chip system with the possibility of automation, offers a notable advantage over existing methods.

4. SIGNIFICANCE AND FUTURE DIRECTIONS

This thesis offers new insights into prostate cancer EV interactions with MP in a microfluidic device. The kinetics data revealed rapid EV binding behaviour, enhancing the understanding of small particle interactions in fluidic systems. To the best of author's knowledge, this study represents the first exploration of prostate-specific EV kinetics with magnetic particles in a microfluidic system.

This study demonstrates the potential of automation using a microfluidic device. The developed system can be operated by setting flow parameters, loading samples, and removing the magnet, eliminating the need for complex workflows typical of conventional laboratory procedures. The resulting microfluidic system can be improved by making it fully automatic by solving engineering challenges, such as automating magnet removal and variable flow settings, to eventually develop it into a practical laboratory tool. The established system could reduce the cost of reagents, improve efficiency and improve the probability of detecting prostate cancer, thus increasing the accuracy of early diagnosis of prostate cancer, which could eventually lead to reduced prostate cancer mortality.

5. CONCLUSIONS

1. Reaction injection moulding of OSTE 322 and OSTE 220 enables fabrication of hermetically sealed OSTE-COC devices with channel geometry defined by a mould or UV mask, and bonding achieved through O_2 plasma treatment, UV light, and heat. Using 140 µm COC film as substrate enables fabrication of an 800 mm-long mixing module connected to a 4 mm-wide magnetic separation module.
2. A passive zig-zag OSTE-COC micro mixer can be used to achieve a relative mixing index of 0.92, that is comparable to the state of art performance [37]. Reducing channel size from 300 µm to 200 µm and increasing flow rate significantly enhances mixing performance, while varying the zigzag angle from 14° to 22.5° does not significantly impact mixing index (p = 0.278).
3. 3D mixing effects, such as vortices, can be attributed to a combination of Dean vortices and the influence of channel sidewalls, as revealed through confocal microscopy for both zig-zag mixer and 1 mm curved channel.
4. The optimal magnetic configuration for capturing magnetic particles was 18 N45 magnets stacked in alternating polarity. Using a setup, with a 4 mm-wide channel, over 98% of 70 µg magnetic particles can be captured while using only 26% of the device's capacity. For higher capacity, the magnetic field strength could be increased by adopting a Halbach array configuration.
5. Extracellular vesicles retain their integrity when subjected to flow rates between 100 and 500 µl/min in the microfluidic magnetic particles capture chamber, as confirmed by qPCR analysis of miRNA375.
6. On-chip capture of LNCaP extracellular vesicles has more consistent western blot signal intensity across a range of flow rates (50–400 µl/min), suggesting that on-chip capture offers a more reliable separation method. However, Off-chip capture yielded higher western blot signal intensity, likely due to longer binding times compared to on-chip.
7. Using a microscopy slide size microfluidic device, CD9-conjugated magnetic particles can be successfully mixed with LNCaP extracellular vesicles, achieving mixing efficiency and binding kinetics comparable to a standard setup. In both configurations, the binding followed asymptotic kinetics described by , reaching saturation within 10 minutes, highlighting the device's suitability for rapid and automated EV capture.

REFERENCES

1. Rimsa, R.; Galvanovskis, A.; Plume, J.; Rumnieks, F.; Grindulis, K.; Paidere, G.; Erentraute, S.; Mozolevskis, G.; Abols, A. Lung on a Chip Development from Off-Stoichiometry Thiol–Ene Polymer. *Micromachines (Basel)* **2021**, *12*, doi:10.3390/mi12050546.
2. Priedols, M.; Paidere, G.; Santos, C. B.; Miscenko, A.; Bergmanis, R. G.; Spule, A.; Bekere, B.; Mozolevskis, G.; Abols, A.; Rimsa, R. Bifurcated Asymmetric Field Flow Fractionation of Nanoparticles in PDMS-Free Microfluidic Devices for Applications in Label-Free Extracellular Vesicle Separation. *Polymers (Basel)* **2023**, *15*, doi:10.3390/polym15040789.
3. Crosby, D.; Bhatia, S.; Brindle, K. M.; Coussens, L. M.; Dive, C.; Emberton, M.; Esener, S.; Fitzgerald, R. C.; Gambhir, S. S.; Kuhn, P.; et al. Early Detection of Cancer. *Science (1979)* **2022**, *375*, doi:10.1126/science.aay9040.
4. Bonifacino, J. S. Vesicular Transport Earns a Nobel. *Trends Cell Biol* **2014**, *24*, 3, doi:10.1016/J.TCB.2013.11.001.
5. Yeo, L. Y.; Chang, H. C.; Chan, P. P. Y.; Friend, J. R. Microfluidic Devices for Bioapplications. *Small* **2011**, *7*, 12–48, doi:10.1002/SMLL.201000946.
6. Shao, H.; Im, H.; Castro, C. M.; Breakefield, X.; Weissleder, R.; Lee, H. New Technologies for Analysis of Extracellular Vesicles. *Chem Rev* **2018**, *118*, 1917–1950, doi:10.1021/acs.chemrev.7b00534.
7. Nawaz, M.; Camussi, G.; Valadi, H.; Nazarenko, I.; Ekström, K.; Wang, X.; Principe, S.; Shah, N.; Ashraf, N. M.; Fatima, F.; et al. The Emerging Role of Extracellular Vesicles as Biomarkers for Urogenital Cancers. *Nature Reviews Urology 2014 11:12* **2014**, *11*, 688–701, doi:10.1038/nrurol.2014.301.
8. Liu, C.; Zhao, J.; Tian, F.; Cai, L.; Zhang, W.; Feng, Q.; Chang, J.; Wan, F.; Yang, Y.; Dai, B.; et al. Low-Cost Thermophoretic Profiling of Extracellular-Vesicle Surface Proteins for the Early Detection and Classification of Cancers. *Nature Biomedical Engineering 2019 3:3* **2019**, *3*, 183–193, doi:10.1038/s41551-018-0343-6.
9. Reátegui, E.; Van Der Vos, K. E.; Lai, C. P.; Zeinali, M.; Atai, N. A.; Aldikacti, B.; Floydjr, F. P.; Khankhel, A. H.; Thapar, V.; Hochberg, F. H.; et al. Engineered Nanointerfaces for Microfluidic Isolation and Molecular Profiling of Tumor-Specific Extracellular Vesicles., doi:10.1038/s41467-017-02261-1.
10. Grant, R.; Ansa-Addo, E.; Stratton, D.; Antwi-Baffour, S.; Jorfi, S.; Kholia, S.; Krige, L.; Lange, S.; Inal, J. A Filtration-Based Protocol to Isolate Human Plasma Membrane-Derived Vesicles and Exosomes from Blood Plasma. *J Immunol Methods* **2011**, *371*, 143–151, doi:10.1016/j.jim.2011.06.024.
11. Ludwig, A. K.; De Miroschedji, K.; Doeppner, T.R.; Börger, V.; Ruesing, J.; Rebmann, V.; Durst, S.; Jansen, S.; Bremer, M.; Behrmann, E.; et al. Precipitation with Polyethylene Glycol Followed by Washing and Pelleting by Ultracentrifugation Enriches Extracellular Vesicles from Tissue Culture Supernatants in Small and Large Scales. *J Extracell Vesicles* **2018**, *7*, doi:10.1080/20013078.2018.1528109.

12. Cheng, S.; Li, Y.; Yan, H.; Wen, Y.; Zhou, X.; Friedman, L.; Zeng, Y. Advances in Microfluidic Extracellular Vesicle Analysis for Cancer Diagnostics. *Lab Chip* 2021, *21*, 3219–3243.
13. Wan, Y.; Cheng, G.; Liu, X.; Hao, S. J.; Nisic, M.; Zhu, C. D.; Xia, Y. Q.; Li, W. Q.; Wang, Z. G.; Zhang, W. L.; et al. Rapid Magnetic Isolation of Extracellular Vesicles via Lipid-Based Nanoprobes. *Nature Biomedical Engineering 2017 1:4* **2017**, *1*, 1–11, doi:10.1038/s41551-017-0058.
14. Chen, W.; Li, H.; Su, W.; Qin, J. Microfluidic Device for On-Chip Isolation and Detection of Circulating Exosomes in Blood of Breast Cancer Patients. *Biomicrofluidics* **2019**, *13*, doi:10.1063/1.5110973/238275.
15. Zhao, Z.; Yang, Y.; Zeng, Y.; He, M. A Microfluidic ExoSearch Chip for Multiplexed Exosome Detection towards Blood-Based Ovarian Cancer Diagnosis. *Lab Chip* **2016**, *16*, 489–496, doi:10.1039/C5LC01117E.
16. Jeong, S.; Park, J.; Pathania, D.; Castro, C. M.; Weissleder, R.; Lee, H. Integrated Magneto-Electrochemical Sensor for Exosome Analysis. *ACS Nano* **2016**, *10*, 1802–1809, doi:10.1021/ACSNANO.5B07584.
17. Clayton, A.; Court, J.; Navabi, H.; Adams, M.; Mason, M. D.; Hobot, J. A.; Newman, G. R.; Jasani, B. Analysis of Antigen Presenting Cell Derived Exosomes, Based on Immuno-Magnetic Isolation and Flow Cytometry. *J Immunol Methods* **2001**, *247*, 163–174, doi:10.1016/S0022-1759(00)00321-5.
18. Chen, J.; Xu, Y.; Lu, Y.; Xing, W. Isolation and Visible Detection of Tumor-Derived Exosomes from Plasma. *Anal Chem* **2018**, *90*, 14207–14215, doi:10.1021/ACS.ANALCHEM.8B03031.
19. Shao, H.; Chung, J.; Lee, K.; Balaj, L.; Min, C.; Carter, B. S.; Hochberg, F. H.; Breakefield, X. O.; Lee, H.; Weissleder, R. Chip-Based Analysis of Exosomal MRNA Mediating Drug Resistance in Glioblastoma. *Nature Communications 2015 6:1* **2015**, *6*, 1–9, doi:10.1038/ncomms7999.
20. Ben Aissa, A.; Araújo, B.; Julián, E.; Zanoni, M. V. B.; Pividori, M. I. Immunomagnetic Separation Improves the Detection of Mycobacteria by Paper-Based Lateral and Vertical Flow Immunochromatographic Assays. *Sensors* **2021**, *21*, 5992, doi:10.3390/S21185992/S1.
21. Yan, L.; Dou, L.; Bu, T.; Huang, Q.; Wang, R.; Yang, Q.; Huang, L.; Wang, J.; Zhang, D. Highly Sensitive Furazolidone Monitoring in Milk by a Signal Amplified Lateral Flow Assay Based on Magnetite Nanoparticles Labeled Dual-Probe. **2018**, doi:10.1016/j.foodchem.2018.04.016.
22. Moyano, A.; Serrano-Pertierra, E.; Salvador, M.; Carlos Martínez-García, J.; Rivas, M.; Carmen Blanco-López, M. Diagnostics Magnetic Lateral Flow Immunoassays., doi:10.3390/diagnostics10050288.
23. Guo, M. T.; Rotem, A.; Heyman, J. A.; Weitz, D. A. Droplet Microfluidics for High-Throughput Biological Assays. *Lab Chip* **2012**, *12*, 2146–2155, doi:10.1039/C2LC21147E.
24. Le, M. C. N.; Fan, Z. H. Exosome Isolation Using Nanostructures and Microfluidic Devices. *Biomedical Materials* **2021**, *16*, 022005, doi:10.1088/1748-605X/ABDE70.

25. Wang, Y.; Li, Q.; Shi, H.; Tang, K.; Qiao, L.; Yu, G.; Ding, C.; Yu, S. Microfluidic Raman Biochip Detection of Exosomes: A Promising Tool for Prostate Cancer Diagnosis. *Lab Chip* **2020**, *20*, 4632–4637, doi:10.1039/d0lc00677g.
26. Freiman, J. M.; Wang, J.; Easterbrook, P. J.; Horsburgh, C. R.; Marinucci, F.; White, L. F.; Kamkamidze, G.; Krajden, M.; Loarec, A.; Njouom, R.; et al. Deriving the Optimal Limit of Detection for an HCV Point-of-Care Test for Viraemic Infection: Analysis of a Global Dataset. *J Hepatol* **2019**, *71*, 62–70, doi:10.1016/j.jhep.2019.02.011.
27. van Meer, B. J.; de Vries, H.; Firth, K. S. A.; van Weerd, J.; Tertoolen, L. G. J.; Karperien, H. B. J.; Jonkheijm, P.; Denning, C.; IJzerman, A. P.; Mummery, C. L. Small Molecule Absorption by PDMS in the Context of Drug Response Bioassays. *Biochem Biophys Res Commun* **2017**, *482*, 323–328, doi:10.1016/J.BBRC.2016.11.062.
28. Kemas, A. M.; Zandi Shafagh, R.; Taebnia, N.; Michel, M.; Preiss, L.; Hofmann, U.; Lauschke, V.M. Compound Absorption in Polymer Devices Impairs the Translatability of Preclinical Safety Assessments. *Adv Healthc Mater* **2023**, doi:10.1002/adhm.202303561.
29. Attia, U. M.; Marson, S.; Alcock, J. R. Micro-Injection Moulding of Polymer Microfluidic Devices. *Microfluid Nanofluidics* **2009**, *7*, 1–28, doi:10.1007/S10404-009-0421-X/TABLES/4.
30. Bajo-Santos, C.; Priedols, M.; Kaukis, P.; Paidere, G.; Gerulis-Bergmanis, R.; Mozolevskis, G.; Abols, A.; Rimsa, R. Extracellular Vesicles Isolation from Large Volume Samples Using a Polydimethylsiloxane-Free Microfluidic Device. *Int J Mol Sci* **2023**, *24*, doi:10.3390/ijms24097971.
31. Nunes, P. S.; Ohlsson, P. D.; Ordeig, O.; Kutter, J. P. Cyclic Olefin Polymers: Emerging Materials for Lab-on-a-Chip Applications. *Microfluid Nanofluidics* **2010**, *9*, 145–161, doi:10.1007/s10404-010-0605-4.
32. Agha, A.; Waheed, W.; Alamoodi, N.; Mathew, B.; Alnaimat, F.; Abu-Nada, E.; Abderrahmane, A.; Alazzam, A. A Review of Cyclic Olefin Copolymer Applications in Microfluidics and Microdevices. *Macromol Mater Eng* **2022**, *307*, doi:10.1002/mame.202200053.
33. Guo, W.; Vilaplana, L.; Hansson, J.; Marco, M.-P.; Van Der Wijngaart, W. Immunoassays on Thiol-Ene Synthetic Paper Generate a Superior Fluorescence Signal. *Biosens Bioelectron* **2020**, *163*, 112279, doi:10.1016/j.bios.2020.112279.
34. Gustafsson, L.; Tasiopoulos, C. P.; Jansson, R.; Kvick, M.; Duursma, T.; Gasser, T. C.; van der Wijngaart, W.; Hedhammar, M. Recombinant Spider Silk Forms Tough and Elastic Nanomembranes That Are Protein-Permeable and Support Cell Attachment and Growth. *Adv Funct Mater* **2020**, *30*, doi:10.1002/adfm.202002982.
35. Errando-Herranz, C.; Saharil, F.; Mola Romero, A.; Sandström, N.; Zandi Shafagh, R.; van der Wijngaart, W.; Haraldsson, T.; Gylfason, K. B.; Sun, Y. S.; Landry, J. P.; et al. Integration of Microfluidics with Grating Coupled Silicon Photonic Sensors by One-Step Combined Photopatterning and Molding of OSTE. *Optics Express, Vol. 21, Issue 18, pp. 21293-21298* **2013**, *21*, 21293–21298, doi:10.1364/OE.21.021293.

36. Sandström, N.; Shafagh, R.Z.; Vastesson, A.; Carlborg, C.F.; Van Der Wijngaart, W.; Haraldsson, T. Reaction Injection Molding and Direct Covalent Bonding of OSTE+ Polymer Microfluidic Devices. *Journal of Micromechanics and Microengineering* **2015**, *25*, 075002, doi:10.1088/0960-1317/25/7/075002.
37. Lee, C. Y.; Wang, W. T.; Liu, C. C.; Fu, L. M. Passive Mixers in Microfluidic Systems: A Review. *Chemical Engineering Journal* 2016, *288*, 146–160.
38. Wang, S.; Huang, X.; Yang, C. Mixing Enhancement for High Viscous Fluids in a Microfluidic Chamber. *Lab Chip* **2011**, *11*, 2081–2087, doi:10.1039/C0LC00695E.
39. Xia, H.M.; Wang, Z.P.; Wang, W.; Fan, W.; Wijaya, A.; Wang, Z.F. Aeroelasticity-Based Fluid Agitation for Lab-on-Chips. *Lab Chip* **2013**, *13*, 1619–1625, doi:10.1039/C3LC41346B.
40. Hashmi, A.; Xu, J. On the Quantification of Mixing in Microfluidics. *J Lab Autom* **2014**, *19*, 488–491, doi:10.1177/2211068214540156.
41. Chen, J. J.; Shie, Y. S. Interfacial Configurations and Mixing Performances of Fluids in Staggered Curved-Channel Micromixers. *Microsystem Technologies* **2012**, *18*, 1823–1833, doi:10.1007/s00542-012-1489-x.
42. Du, Y.; Zhang, Z.; Yim, C. H.; Lin, M.; Cao, X. Evaluation of Floor-Grooved Micromixers Using Concentration-Channel Length Profiles. *Micromachines 2010, Vol. 1, Pages 19-33* **2010**, *1*, 19–33, doi:10.3390/MI1010019.
43. Rösing, W.; Schildhauer, T.; König, J.; Cierpka, C. Passive Control of the Concentration Boundary Layer in Microfluidic Fuel Cells Using Dean Vortices. *Microfluid Nanofluidics* **2019**, *23*, doi:10.1007/s10404-019-2274-2.
44. Cosentino, A.; Madadi, H.; Vergara, P.; Vecchione, R.; Causa, F.; Netti, P. A. An Efficient Planar Accordion-Shaped Micromixer: From Biochemical Mixing to Biological Application. *Scientific Reports 2015 5:1* **2015**, *5*, 1–10, doi:10.1038/srep17876.
45. Fellouah, H.; Castelain, C.; Ould El Moctar, A.; Peerhossaini, H. A Criterion for Detection of the Onset of Dean Instability in Newtonian Fluids. *European Journal of Mechanics – B/Fluids* **2006**, *25*, 505–531, doi:10.1016/J.EUROMECHFLU.2005.11.002.
46. Petkovic, K.; Metcalfe, G.; Chen, H.; Gao, Y.; Best, M.; Lester, D.; Zhu, Y. Rapid Detection of Hendra Virus Antibodies: An Integrated Device with Nanoparticle Assay and Chaotic Micromixing. *Lab Chip* **2017**, *17*, 169–177, doi:10.1039/c6lc01263a.
47. Caltag Exosome-Human CD63 Isolation/Detection (from Cell Culture Media) Protocol for Use in Flow Cytometry Product Description.
48. Technologies, L. *Exosome-Human CD9 Isolation (from Cell Culture) Pre-Enriched Exosome Sample Input*; 2014.

ACKNOWLEDGEMENTS

The author wishes to express sincere gratitude to the Latvian Biomedical Research and Study Centre, particularly to **Edgars Endzelins** and the **Aija Line** group, for their invaluable contributions in producing extracellular vesicles (EVs) and magnetic particle (MP) conjugate nanobodies. Their assistance in conducting experiments, including iron content analysis, Western blot, and qPCR measurements, as well as performing the standard assay control experiments, was instrumental to this research.

The author is also thankful to colleagues at **Cellbox Labs** and the Institute of **Solid State Physics** for their insightful discussions and guidance regarding the fabrication and testing processes of the microfluidic devices, most notably **Roberts Rimsa** for the PhD mentorship.

Additionally, the author acknowledges the University of Latvia for providing the opportunity to conduct PhD research within the "Natural Sciences (Physics, Astronomy and Mechanics) Academic Doctor" program.

Finally, the author expresses appreciation to the founding agency for their support throughout this research project: Project was funded by European Regional Development Fund (ERDF), Measure 1.1.1.1 "Support for applied research" No 1.1.1.1/20/A/045, "Development of a novel microfluidic device for label-free quantification of prostate cancer-derived extracellular vesicles and analysis of their RNA content (PROCEX)" The financial support of Latvian Council of Science project VPP-EM-FOTONIKA-2022/1-0001 "Smart Materials, Photonics, Technologies, and Engineering Ecosystems is apricated.